Atmospheric Research 205 (2018) 60–69

Contents lists available at ScienceDirect

Atmospheric Research

journal homepage: www.elsevier.com/locate/atmosres

# Contributions of natural climate changes and human activities to the trend of extreme precipitation

Lu Gao[a,b,c,d,*], Jie Huang[b], Xingwei Chen[a,b,c,d], Ying Chen[a,b,c,d], Meibing Liu[a,b,c,d]

[a] Institute of Geography, Fujian Normal University, Fuzhou, China
[b] College of Geographical Science, Fujian Normal University, Fuzhou, China
[c] Fujian Provincial Engineering Research Center for Monitoring and Assessing Terrestrial Disasters, Fujian Normal University, Fuzhou, China
[d] State Key Laboratory of Subtropical Mountain Ecology (Funded by Ministry of Science and Technology and Fujian Province), Fujian Normal University, Fuzhou, China

ARTICLE INFO

*Keywords:*
Nonstationarity
Precipitation
Trend
Climate change
Human activity
Risk

ABSTRACT

This study focuses on the analysis of the nonstationarity characteristics of extreme precipitation and their attributions in the southeastern coastal region of China. The maximum daily precipitation (MDP) series is extracted from observations at 79 meteorological stations in the study area during the first flood season (April–June) from 1960 to 2012. The trends of the mean (Mn) and variance (Var) of MDP are detected using the Generalized Additive Models for Location, Scale, and Shape parameters (GAMLSS) and Mann-Kendall test. The contributions of natural climate change and human activities to the Mn and Var changes of MDP are investigated using six large-scale circulation variables and emissions of four greenhouse gases based on GAMLSS and a contribution analysis method. The results demonstrate that the nonstationarity of extreme precipitation on local scales is significant. The Mn and Var of extreme precipitation increase in the north of Zhejiang, the middle of Fujian, and the south of Guangdong. In general, natural climate change contributes more to Mn from 1960 to 2012 than to Var. However, human activities cause a greater Var in the rapid socioeconomic development period (1986–2012) than in the slow socioeconomic development period (1960–1985), especially in Zhejiang and Guangdong. The community should pay more attention to the possibility of extreme precipitation events and associated disasters triggered by human activities.

## 1. Introduction

Extreme precipitation leads to serious disasters that cause large human and economic losses because it tends to trigger natural hazards such as floods, landslides, and debris flows (Easterling et al., 2000). The global increase in the frequency and intensity of extreme precipitation events has been observed in numerous studies (e.g., Alexander et al., 2006; Coumou and Rahmstorf, 2012; Ingram, 2016; IPCC, 2013). Many previous studies showed that China experiences a significant increase in the extreme precipitation, in particular northwestern and southeastern China, during the rainy season from April to September (e.g., Fu et al., 2013; Ning and Qian, 2009; Wang and Zhou, 2005; Xu et al., 2011; You et al., 2011; Zhai et al., 2005; Zhang et al., 2009, 2008).

The reasons behind the extreme precipitation changes have been widely discussed in the past decades. The IPCC (2013) believes that extreme precipitation events can inevitably be attributed to the combined influence of natural and human factors. Specifically speaking, global warming and anthropogenic aerosols are considered to be the major components affecting extreme precipitation changes (e.g., Liu et al., 2015; Qin et al., 2005; Rosenfeld et al., 2008; Wang, 2015). Ohba et al. (2015) concluded that extreme precipitation is significantly influenced by multiple effects of the East Asian monsoon, the El Niño/Southern Oscillation (ENSO), and the Pacific Ocean circulation in East Asia. Anomalies of the sea surface temperature of the tropical Pacific and India oceans were found to affect the precipitation intensity and typhoon paths in East Asia (Du et al., 2011; Ohba, 2013; Xie et al., 2009). The ENSO, Pacific Decadal Oscillation (PDO), and Southern Oscillation (SO) are found to be significantly associated with extreme precipitation in most regions of China, especially in southern China (e.g., Chan and Zhou, 2005; Wan et al., 2013).

Many studies pointed out that anthropogenic (human activity impacts) contribution causes more intense extreme precipitation events (e.g., Fischer and Knutti, 2015; Min et al., 2011). The effect of human activity on climate change is mainly reflected by fossil fuels, greenhouse gases from agricultural and industrial activities, land use and land cover change, and aerosol emissions (Ding, 2008). Gao et al. (2002) showed that the precipitation amount and intensity significantly increased in the Yangtze River Basin and eastern China at a double $CO_2$

* Corresponding author at: Institute of Geography, Fujian Normal University, Fuzhou, China.
*E-mail address:* l.gao@foxmail.com (L. Gao).

https://doi.org/10.1016/j.atmosres.2018.02.006
Received 3 August 2017; Received in revised form 7 February 2018; Accepted 12 February 2018
Available online 13 February 2018
0169-8095/ 

condition based on a nested Regional Climate Model. Land use changes affect the global and regional climate by changing the atmospheric moisture and energy balance of the ecosystem (Fu, 2003; Liu et al., 2011; Salazar et al., 2015).

However, particular contributions are still debated. It is known that precipitation and large-scale circulations, anthropogenic aerosols, and synoptic processes have a complex relationship, in particular on regional scales (Ohba et al., 2015; Wang, 2015). Under these conditions, meteorological and hydrological series show significant nonstationarity characteristics. Thus, the conventional stationary hypothesis is questionable to assess flood risk as well as to design hydraulic engineering projects in a changing environment (Beguería et al., 2011; Gilroy and McCuen, 2012; Milly et al., 2008; Zhang et al., 2014). The changes of the mean (Mn) and variance (Var) of the data series primarily show nonstationarity (Khaliq et al., 2006). The remarkable change in the intensity and frequency of an extreme precipitation event could be due to a small change in the mean (Mearns et al., 1984). The effect of the variance is greater than the average state of the climate, which suggests that an increased variance possibly leads to more extreme precipitation, even when the climate is in an invariable mean state (Katz and Brown, 1992).

The southeastern coastal region of China, including the Shanghai City, Zhejiang, Fujian, Guangdong, and Hainan provinces (excluding the South China Sea Islands), is located in a typical subtropical monsoon climate zone. It is an economically developed area with a high population density and a high concentration of wealth (Fig. 1). However, natural disasters, such as floods, typhoons, and mountain torrents, often occur in this region. Based on preliminary statistics, > 182 extreme precipitation events occurred in the Fujian Province alone, which caused > 2000 deaths from 1950 to 2000 (Song and Cai, 2007).

The investigation of the variation of extreme precipitation and its possible impact factors is therefore of great importance and helpful for the risk assessment of natural disasters and water resource management in the southeastern coastal region of China. This study therefore focuses on the extreme precipitation in the first flood season (April to June). The objectives include: 1) detecting the nonstationarity characteristics of extreme precipitation by analyzing the trends of the mean and variance of the maximum daily precipitation series (MDP) and 2) investigating the contributions of natural climate change and human activities to extreme precipitation based on a nonstationarity model, the Generalized Additive Models for Location, Scale, and Shape parameters (GAMLSS). Six large-scale circulation indices and emissions of four greenhouse gases were selected to represent natural climate change (non-anthropogenic) and human activity effects (anthropogenic), respectively. The remainder of this paper is structured as follows. Section 2 describes the datasets. The analysis methods are presented in Section 3, and the results are presented in Section 4. Finally, the discussion and conclusions are presented in Section 5.

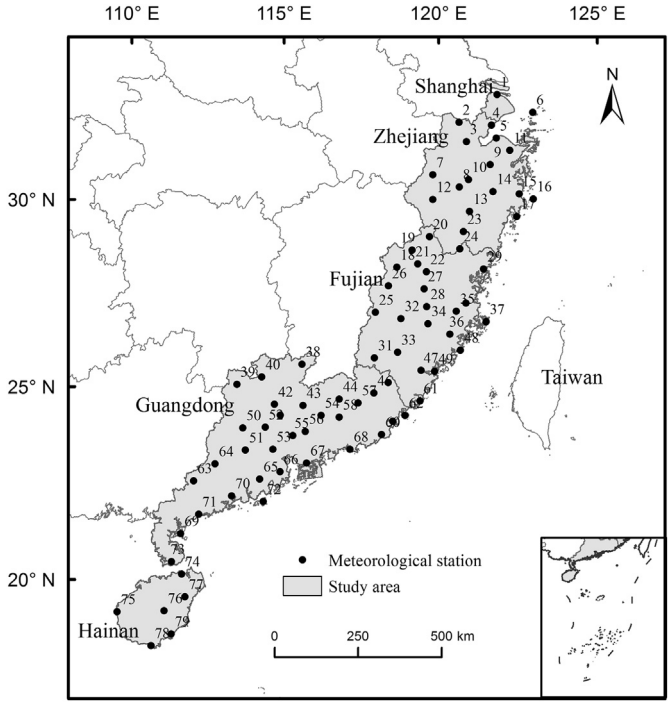


**Fig. 1.** Location of meteorological stations and study area.

## 2. Data

### 2.1. Meteorological observations

Seventy-nine meteorological stations conducting long-term consecutive measurements (no gaps exceeding two consecutive weeks) in the southeastern coastal region of China were selected from the China Meteorological Data Sharing Service System of the National Meteorological Information Center (http://data.cma.cn/; Fig. 1, Table 1). The daily precipitation records in the first flood season (April to June) during 1960 to 2012 were extracted for the analysis. An extreme precipitation series (hereafter MDP) was constructed for each station by retrieving the maximum daily precipitation from April to June for each year. The MDP series was further used in GAMLSS as a response variable. As stated above, Mn and Var are the most important indicators reflecting the stability and variability of a trend in a continuous data series. Therefore, the present study investigates the nonstationarity characteristics of MDP by detecting the trends of Mn and Var. However, it is worth noting that the trends of Mn and Var were not examined straightforward by using Mann-Kendall test (MK). Previous studies have pointed out that the conventional methods (e.g., linear regression and MK) are problematic to detect the trends in nonstationarity conditions (e.g., L. Gao et al., 2017). Thus, this study investigated the trends of Mn and Var in two steps with considering nature climate change and human activities. Two fitting coefficients, which stand for Mn and Var were returned by GAMLSS for each station and each year. Then, the variation of Mn and Var were explored by detected the trends of these two coefficient series based on MK.

### 2.2. Large-scale circulations and emissions of greenhouse gases

There is no doubt that climate change and human activity interact. However, to directly distinguish these two impact factors, we selected six large-scale circulation indices representing the natural climate change (non-anthropogenic) and emission of four greenhouse gases and thus the human activity effects (anthropogenic) based on previous studies. The natural climate change factors are the West Pacific Pattern Teleconnection Index (WP), North Pacific Oscillation Index (NPO), Pacific Decadal Oscillation (PDO), Arctic Oscillation Index (AO), Southern Oscillation (SO), and sea surface temperature anomaly in the eastern tropical Pacific Ocean (150°–90°W, 5°S–5°N, Nino3), which were derived from the Climate Diagnostics and Prediction Division of the National Climate Center of China (http://ncc.cma.gov.cn). The four greenhouse gases are $CO_2$, $CH_4$, $SO_2$, and $N_2O$. The emission data were derived from the Emission Database for Global Atmospheric Research (EDGAR v4.2) of the Joint Research Center of the European Commission (http://edgar.jrc.ec.europa.eu/overview.php?v=42). The $0.1^\circ \times 0.1^\circ$ data were adjusted for individual stations based on their coordinates. Small-scale mismatch was ignored, which did not affect the analysis in this study. To reduce the complexity of climate change and diversity of greenhouse gases, an integrated index of natural climate change (CI) and human activities (HI) was constructed based on principal component analysis (PCA). This process does not only reflect the comprehensive impact of multiple climate change or human factors on the MDP but also reduces the dimensions of variables and improves

**Table 1**
Information of meteorological stations.

| No. | Station | Latitude | Longitude | No. | Station | Latitude | Longitude |
|---|---|---|---|---|---|---|---|
| 1 | Baoshan | 31.42 | 121.47 | 41 | Fogang | 23.87 | 113.53 |
| 2 | Huzhou | 30.88 | 120.12 | 42 | Yingde | 24.17 | 113.40 |
| 3 | Hangzhou | 30.33 | 120.23 | 43 | Xinfeng | 24.05 | 114.20 |
| 4 | Pinghu | 30.63 | 121.10 | 44 | Longchuan | 24.10 | 115.25 |
| 5 | Cixi | 30.27 | 121.17 | 45 | Dapu | 24.35 | 116.70 |
| 6 | Shengsi | 30.73 | 122.45 | 46 | Meixian | 24.13 | 116.25 |
| 7 | Chun'an | 29.62 | 119.02 | 47 | Zhangzhou | 24.53 | 117.68 |
| 8 | Jinhua | 29.17 | 119.75 | 48 | Chongwu | 24.88 | 118.90 |
| 9 | Shengxian | 29.60 | 120.82 | 49 | Xiamen | 24.45 | 118.07 |
| 10 | Yiwu | 29.32 | 120.07 | 50 | Guangning | 23.63 | 112.43 |
| 11 | Yinxian | 29.87 | 121.50 | 51 | Zhaoqing | 23.05 | 112.45 |
| 12 | Quzhou | 28.97 | 118.88 | 52 | Qingyuan | 23.60 | 113.07 |
| 13 | Lishui | 28.47 | 119.92 | 53 | Guangzhou | 23.00 | 113.22 |
| 14 | Xianju | 28.87 | 120.73 | 54 | Dongyuan | 23.73 | 114.68 |
| 15 | Hongjia | 28.67 | 121.50 | 55 | Zengcheng | 23.30 | 113.82 |
| 16 | Dachendao | 28.45 | 121.88 | 56 | Huiyang | 23.37 | 114.18 |
| 17 | Yuhuan | 28.08 | 121.28 | 57 | Wuhua | 23.93 | 115.77 |
| 18 | Shaowu | 27.33 | 117.47 | 58 | Zijin | 23.63 | 115.18 |
| 19 | Wuyishan | 27.72 | 118.00 | 59 | Shantou | 23.33 | 116.67 |
| 20 | Pucheng | 28.00 | 118.58 | 60 | Huilai | 23.03 | 116.30 |
| 21 | Jianyang | 27.33 | 118.10 | 61 | Dongshan | 23.75 | 117.52 |
| 22 | Jian'ou | 27.08 | 118.32 | 62 | Nan'ao | 23.43 | 117.03 |
| 23 | Yunhe | 27.97 | 119.62 | 63 | Xinyi | 22.37 | 110.93 |
| 24 | Shouning | 27.53 | 119.42 | 64 | Luoding | 22.77 | 111.57 |
| 25 | Ninghua | 26.23 | 116.63 | 65 | Taishan | 22.27 | 112.77 |
| 26 | Taining | 26.88 | 117.13 | 66 | Zhongshan | 22.40 | 113.35 |
| 27 | Nanping | 26.65 | 118.17 | 67 | Shenzhen | 22.55 | 114.12 |
| 28 | Youxi | 26.17 | 118.15 | 68 | Shanwei | 22.77 | 115.37 |
| 29 | Xiapu | 26.88 | 120.00 | 69 | Zhanjiang | 21.03 | 110.47 |
| 30 | Fuzhou | 26.08 | 119.30 | 70 | Yangjiang | 21.90 | 111.95 |
| 31 | Shanghang | 25.05 | 116.42 | 71 | Dianbai | 21.50 | 111.00 |
| 32 | Yong'an | 25.97 | 117.35 | 72 | Shangchuandao | 21.68 | 112.80 |
| 33 | Longyan | 25.10 | 117.10 | 73 | Xuwen | 20.33 | 110.17 |
| 34 | Jiuxianshan | 25.72 | 118.10 | 74 | Haikou | 20.00 | 110.42 |
| 35 | Pingnan | 25.92 | 118.98 | 75 | Dongfang | 19.13 | 108.63 |
| 36 | Xianyou | 25.35 | 118.68 | 76 | Qiongzhong | 19.10 | 109.88 |
| 37 | Pingtan | 25.50 | 119.78 | 77 | Qionghai | 19.42 | 110.47 |
| 38 | Nanxiong | 25.13 | 114.32 | 78 | Sanya | 18.23 | 109.48 |
| 39 | Lianxian | 24.78 | 112.38 | 79 | Lingshui | 18.50 | 110.03 |
| 40 | Shaoguan | 24.92 | 113.12 | | | | |

the efficiency of GAMLSS (L. Gao et al., 2017).

## 3. Methods

### 3.1. GAMLSS model

To simulate the linear and nonlinear relations between response and explanatory variables under nonstationarity conditions, the Generalized Additive Models for Location, Scale, and Shape parameters (GAMLSS) was developed by Rigby and Stasinopoulos (2005). The ability of introducing multiple explanatory variables is the outstanding advantage of GAMLSS. Previous studies have shown that GAMLSS was suitable for the trend analysis of precipitation, temperature, and runoff series (e.g., L. Gao et al., 2017; Villarini et al., 2010; Zhang et al., 2015). GAMLSS has two different types, full parametric and semi-parametric model. In order to gain the parametric, nonparametric and random-effects terms, the semi-parametric GAMLSS model is applied here. The independent observations at the time moment $i$ ($i = 1, 2, \ldots, n$), MDP in this study (defined as $y_i$), are subject to the distribution of $f_y(y_i|\theta_i)$, where, $\theta_{ik} = (\theta_{i1},\theta_{i2}, \ldots, \theta_{ip})$ represent the $p$ parameters vector (position, scale, and shape), $k = 1, 2, \ldots, p$. $p$ is generally less than four. Thus, a nonlinear semi-parametric GAMLSS is defined as follows:

$$g_k(\theta_k) = \varnothing_k \beta_k + \sum_{j=1}^{m} h_{jk}(x_{jk}) \quad (1)$$

where $\theta_k$ is the vector of $k$ *distribution parameter* with length $n$; $\varnothing_k$ is the explanatory variable (i.e., the time, CI, and HI) in the $n \times m$ matrix; $\beta_k$ is the parameter vector of length $m$; and $h_{jk}(.)$ represents the joint function (the cubic spline function is applied here) between the distribution parameters and explanatory variables $x_{jk}$. More details about the GAMLSS definition could be found in Rigby and Stasinopoulos (2005).

In this study, forty-eight different linear and nonlinear (i.e., stationarity and nonstationarity) relationships were considered between MDP and CI and HI. For example, the nonstationary model as a function of MDP and CI/HI varies with time or as function of MDP and the combined CI and HI vary with time. All these functions were evaluated based on seven widely used distribution functions: Gamma (GA), Lognormal (LOGNO), Generalized gamma (GG), Inverse gamma (IGA), Inverse Gaussian (IG), Reverse Gumbel (RG), and Skew Normal Type 2 (SN2). The optimal distribution with the highest goodness-of-fit performance with the minimum Akaike information criterion (AIC) value was selected. The specific information for all functions could be found in Rigby and Stasinopoulos (2009). Here, we could like to explain specifically how to assess the contribution of CI or HI to MDP as well as the trends of Mn and Var. There are two parameters returned from GAMLSS based on the selected function (best function with minimum AIC from the 48 functions) for each station and each year. These two parameters series standing for Mn and Var were further detected the trends using MK. As well-known, location parameter in a distribution function is related to the order of magnitude of data while scale parameter is correlated to the variability of data. Thus, the fitting coefficients containing location and scale parameter information modeled by

GAMLSS could be used for assessing the impacts of CI and HI. In short, GAMLSS modeled the trends of Mn and Var for each station. The nonparametric MK was used to quantify the significance of the trends. In addition, the fitting coefficient was used to determine the contributions of CI and HI to the trend changes of Mn and Var. The model was accomplished using a GAMLSS code package in R@ (Rigby and Stasinopoulos, 2009).

### 3.2. Contribution analysis

Karl and Knight (1998) proposed a contribution analysis method to assess the precipitation increment in the United States. Based on this method, the contributions of natural climate change and human activity to the Mn and Var trends of MDP are discussed here after calculating the proportion. Here, we take a certain station as the example to illustrate how to determine the impacts of CI and HI on Mn of MDP. The procedures are as follows:

$$b_c = p_m(T_c) \tag{2}$$

where $b_c$ is the contribution of CI to the Mn trend of MDP. $T_c$ represents the Mn trend of CI. It is the slope of the linear regression of CI trends returned by GAMLSS. The $p_m$ is the mean value of Mn trends results from GAMLSS. The function could be simple multiplication. The contribution of HI ($b_h$) can be calculated as:

$$b_\mathrm{h} = b - b_c \tag{3}$$

where $b$ is the total trend of MDP by summing the Mn trends of CI and HI. The contribution of CI and HI can be compared:

$$r = \frac{|b_\mathrm{c}| - |b_\mathrm{h}|}{p_m} \times 100\% \tag{4}$$

where $r$ is the percentage difference (relative contribution rate). A positive $r$ indicates that the contribution of CI is greater than HI to the Mn trend of MDP while a negative $r$ indicates the less contribution of CI than HI. In the same way, the impacts CI and HI on Var of MDP can be calculated for each station. The contributions can also be analyzed in different time series.

## 4. Results

### 4.1. Trends of Mn and Var of MDP

Fig. 2 and Table 2 illustrate the MK trends for Mn and Var of MDF based on GAMLSS at different confidence levels from 1960 to 2012. In total, 15 stations have significant decreasing Mn trends in the study area. Thirteen stations show the most significant decreasing trend (99% confidence level); they are mainly located in the east of Guangdong, northern Fujian, and in the west of Hainan. However, two other stations show increasing trends. In total, 17 stations with remarkable increasing trends are widely distributed, from Zhejiang to Guangdong. Among them, thirteen stations, showing the most significant increasing trends (99%), are located in the north of Zhejiang, middle of Fujian, and south of Guangdong. Guangdong has the most stations (seven stations) with significant increasing trends. Forty-seven stations did not show any trend. That is to say, the Mn of MDP of 40.5% of the stations have significantly varies.

**Table 2**
Station statistics of MK trends for Mn and Var of MDP from 1960 to 2012.

| Confidence level | Mn | | | Var | | |
|---|---|---|---|---|---|---|
| | 99% | 95% | 90% | 99% | 95% | 90% |
| Decreasing trend | 13 | 2 | 0 | 2 | 2 | 3 |
| Increasing trend | 13 | 2 | 2 | 12 | 0 | 0 |

One station in Zhejiang (No. 9) and one station in Hainan (No. 78) show a significant decrease of Var at the 99% confidence level, respectively. Two other stations show decreasing trends at the 95% confidence level; they are located in Fujian (No. 30) and Guangdong (No. 68), respectively. Three stations distributed in Zhejiang (No. 16), Guangdong (No. 40) and Hainan (No. 79) display decreasing trends at the 90% confidence level. Twelve stations have significant increasing trends. Zhejiang, Fujian, and Guangdong include three stations, respectively. In general, the increase of Var is much more significant than the decrease. Sixty stations show neither significant increase nor decrease of Var.

### 4.2. Attribution analysis

A certain distribution with the highest goodness-of-fit performance was selected for each site based on the AIC value. The IGA was selected at most sites (23 sites), and GA performed best at nine sites. The IG and SN2 were selected at 16 sites, while LOGNO and RG were selected at six sites. The GG was only chosen at three sites. The residual moments and computed Filliben coefficients showed that the GAMLSS model results are encouraging (Table 3). Normally, the Filliben coefficients are higher than 0.95, indicating that the fits of GAMLSS meet the analysis requirements (Gu et al., 2016). The Filliben coefficient ranges from 0.976 to 0.997, with an average value of 0.991, which indicates that the residuals of GAMLSS follow the normal distribution very well. The average Mn and Var of the residuals are −0.021 and 1.047, respectively. They are very close to 0.0 and 1.0, which indicates insignificant deviations from normality (Table 3). The fitting coefficient for the location and scale parameters was simulated using CI and HI as the explanatory variables in GAMLSS.

A positive fitting coefficient reflects the increasing impact of CI/HI

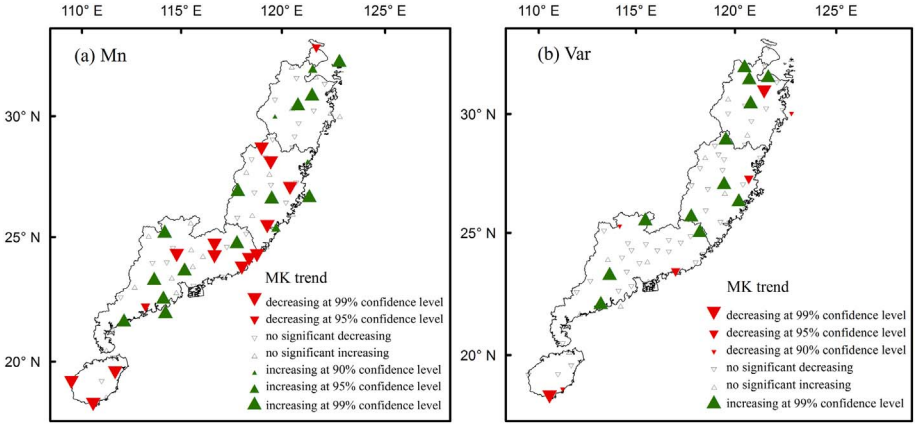


**Fig. 2.** Spatial distribution of MK trends for Mn and Var of MDP from 1960 to 2012.

**Table 3**
Residual moments for GAMLSS model and computed Filliben coefficient for all 79 sites.

| No. | Station | Distribution | AIC | Mean | Variance | Skewness | Kurtosis | Filliben |
|---|---|---|---|---|---|---|---|---|
| 1 | Baoshan | IGAMMA | 484.98 | 0.002 | | −0.21 | 2.58 | 0.996 |
| 2 | Huzhou | LOGNO | 477.51 | 0.008 | 1.02 | −0.43 | 3.22 | 0.988 |
| 3 | Hangzhou | SN2 | 480.34 | 0.003 | 1.01 | −0.03 | 1.88 | 0.984 |
| 4 | Pinghu | IG | 483.99 | 0.013 | 1.03 | −0.27 | 2.48 | 0.989 |
| 5 | Cixi | GA | 480.14 | −0.258 | 1.23 | 0.49 | 2.92 | 0.986 |
| 6 | Shengsi | IG | 490.80 | −0.010 | 1.02 | −0.27 | 2.62 | 0.992 |
| 7 | Chun'an | GA | 519.73 | −0.033 | 1.00 | 0.15 | 2.10 | 0.988 |
| 8 | Jinhua | GA | 488.00 | 0.000 | 1.02 | −0.09 | 2.52 | 0.997 |
| 9 | Shengxian | IGAMMA | 464.51 | 0.055 | 1.05 | 0.08 | 3.01 | 0.995 |
| 10 | Yiwu | RG | 491.20 | −0.022 | 1.02 | 0.06 | 2.50 | 0.995 |
| 11 | Yinxian | RG | 465.66 | −0.030 | 1.01 | −0.13 | 2.53 | 0.992 |
| 12 | Quzhou | IG | 512.17 | 0.009 | 1.02 | 0.01 | 2.72 | 0.997 |
| 13 | Lishui | GA | 474.36 | 0.002 | 1.02 | 0.00 | 2.57 | 0.992 |
| 14 | Xianju | IG | 475.35 | 0.009 | 1.02 | −0.23 | 2.63 | 0.994 |
| 15 | Hongjia | LOGNO | 459.12 | −0.048 | 1.02 | −0.34 | 2.33 | 0.986 |
| 16 | Dachendao | SN2 | 494.43 | −0.114 | 1.15 | 0.26 | 2.05 | 0.985 |
| 17 | Yuhuan | IGAMMA | 490.86 | 0.001 | 1.02 | −0.07 | 2.37 | 0.995 |
| 18 | Shaowu | RG | 514.00 | −0.027 | 1.02 | −0.10 | 2.75 | 0.994 |
| 19 | Wuyishan | IGAMMA | 546.45 | −0.001 | 1.02 | 0.55 | 3.01 | 0.982 |
| 20 | Pucheng | IGAMMA | 514.35 | 0.008 | 1.01 | −0.18 | 2.29 | 0.992 |
| 21 | Jianyang | IGAMMA | 506.20 | −0.004 | 1.02 | 0.28 | 2.96 | 0.990 |
| 22 | Jian'ou | SN2 | 513.74 | −0.174 | 1.24 | 0.32 | 2.43 | 0.983 |
| 23 | Yunhe | SN2 | 489.75 | 0.007 | 1.02 | −0.24 | 2.35 | 0.994 |
| 24 | Shouning | IGAMMA | 493.59 | 0.017 | 1.00 | −0.47 | 2.69 | 0.988 |
| 25 | Ninghua | IGAMMA | 526.03 | −0.001 | 1.02 | 0.32 | 3.28 | 0.991 |
| 26 | Taining | IG | 529.53 | 0.000 | 1.02 | −0.12 | 3.12 | 0.991 |
| 27 | Nanping | SN2 | 513.86 | 0.000 | 1.02 | 0.25 | 2.60 | 0.994 |
| 28 | Youxi | SN2 | 480.83 | −0.205 | 1.33 | 0.36 | 2.44 | 0.991 |
| 29 | Xiapu | SN2 | 494.95 | 0.000 | 1.02 | 0.07 | 1.89 | 0.985 |
| 30 | Fuzhou | GG | 479.95 | −0.004 | 1.01 | 0.25 | 2.65 | 0.991 |
| 31 | Shanghang | IGAMMA | 503.44 | 0.007 | 1.01 | −0.08 | 3.06 | 0.993 |
| 32 | Yong'an | IGAMMA | 494.75 | −0.026 | 1.04 | −0.08 | 2.42 | 0.995 |
| 33 | Longyan | IGAMMA | 500.11 | −0.109 | 1.13 | 0.22 | 2.22 | 0.989 |
| 34 | Jiuxianshan | IG | 488.06 | −0.163 | 1.56 | 0.20 | 2.38 | 0.986 |
| 35 | Pingnan | SN2 | 529.24 | −0.188 | 1.22 | 0.44 | 2.31 | 0.982 |
| 36 | Xianyou | SN2 | 529.87 | −0.186 | 1.25 | 0.32 | 2.36 | 0.976 |
| 37 | Pingtan | SN2 | 550.73 | −0.004 | 1.02 | 0.26 | 2.22 | 0.988 |
| 38 | Nanxiong | IG | 492.12 | −0.035 | 0.99 | 0.36 | 2.18 | 0.983 |
| 39 | Lianxian | GG | 471.64 | −0.054 | 1.14 | 0.17 | 2.80 | 0.993 |
| 40 | Shaoguan | IG | 522.10 | 0.000 | 1.02 | 0.11 | 2.42 | 0.992 |
| 41 | Fogang | RG | 568.05 | 0.002 | 1.04 | 0.09 | 2.78 | 0.992 |
| 42 | Yingde | IGAMMA | 542.89 | 0.000 | 1.02 | 0.17 | 2.34 | 0.993 |
| 43 | Xinfeng | IGAMMA | 531.93 | −0.078 | 1.08 | −0.28 | 2.83 | 0.993 |
| 44 | Longchuan | GA | 522.54 | 0.000 | 1.02 | −0.18 | 2.13 | 0.989 |
| 45 | Dapu | IGAMMA | 505.94 | 0.000 | 1.02 | 0.20 | 3.06 | 0.993 |
| 46 | Meixian | IGAMMA | 507.54 | 0.001 | 1.02 | −0.12 | 2.87 | 0.994 |
| 47 | Zhangzhou | IGAMMA | 533.21 | 0.001 | 1.02 | −0.12 | 2.66 | 0.993 |
| 48 | Chongwu | SN2 | 536.35 | 0.000 | 1.02 | 0.02 | 2.26 | 0.991 |
| 49 | Xiamen | GG | 528.64 | 0.016 | 1.01 | 0.02 | 2.31 | 0.994 |
| 50 | Guangning | IGAMMA | 499.57 | 0.007 | 1.01 | −0.16 | 2.71 | 0.996 |
| 51 | Zhaoqing | IG | 534.98 | 0.017 | 1.03 | 0.15 | 2.29 | 0.995 |
| 52 | Qingyuan | IGAMMA | 568.89 | 0.019 | 0.99 | −0.06 | 2.61 | 0.994 |
| 53 | Guangzhou | RG | 537.65 | −0.001 | 1.02 | 0.22 | 2.71 | 0.994 |
| 54 | Dongyuan | IGAMMA | 550.94 | 0.001 | 1.02 | −0.04 | 2.35 | 0.995 |
| 55 | Zengcheng | SN2 | 526.21 | 0.006 | 1.02 | 0.03 | 2.04 | 0.984 |
| 56 | Huiyang | GA | 547.50 | 0.001 | 1.02 | 0.00 | 2.13 | 0.994 |
| 57 | Wuhua | IGAMMA | 506.09 | −0.001 | 1.02 | 0.17 | 2.60 | 0.996 |
| 58 | Zijin | RG | 523.62 | 0.015 | 1.03 | 0.03 | 2.19 | 0.993 |
| 59 | Shantou | IG | 560.74 | 0.001 | 1.02 | −0.25 | 2.58 | 0.991 |
| 60 | Huilai | GA | 579.80 | −0.001 | 1.02 | 0.16 | 2.02 | 0.987 |
| 61 | Dongshan | IGAMMA | 548.61 | −0.007 | 1.03 | −0.32 | 3.12 | 0.991 |
| 62 | Nan'ao | IG | 566.07 | 0.000 | 1.02 | −0.03 | 2.27 | 0.990 |
| 63 | Xinyi | IG | 550.49 | −0.017 | 1.01 | 0.01 | 2.03 | 0.991 |
| 64 | Luoding | GA | 467.58 | 0.000 | 1.02 | −0.07 | 3.12 | 0.993 |
| 65 | Taishan | IG | 573.89 | −0.063 | 0.97 | 0.35 | 2.59 | 0.993 |
| 66 | Zhongshan | SN2 | 573.66 | 0.012 | 1.03 | −0.22 | 2.45 | 0.993 |
| 67 | Shenzhen | LOGNO | 573.41 | 0.075 | 1.01 | −0.22 | 2.30 | 0.994 |
| 68 | Shanwei | LOGNO | 585.01 | 0.061 | 1.02 | 0.09 | 2.54 | 0.990 |
| 69 | Zhanjiang | IGAMMA | 561.39 | 0.007 | 1.01 | −0.10 | 2.55 | 0.994 |
| 70 | Yangjiang | SN2 | 629.95 | −0.151 | 1.17 | 0.34 | 2.15 | 0.983 |
| 71 | Dianbai | IG | 559.71 | −0.034 | 1.00 | −0.05 | 2.14 | 0.994 |
| 72 | Shangchuandao | LOGNO | 611.81 | −0.015 | 1.02 | 0.07 | 2.78 | 0.994 |
| 73 | Xuwen | IGAMMA | 548.52 | −0.004 | 1.02 | −0.26 | 2.61 | 0.991 |
| 74 | Haikou | SN2 | 534.01 | −0.019 | 1.00 | 0.35 | 2.01 | 0.979 |

(*continued on next page*)

**Table 3** (*continued*)

| No. | Station | Distribution | AIC | Mean | Variance | Skewness | Kurtosis | Filliben |
|---|---|---|---|---|---|---|---|---|
| 75 | Dongfang | SN2 | 538.22 | 0.000 | 1.02 | −0.24 | 2.08 | 0.984 |
| 76 | Qiongzhong | IG | 516.65 | 0.006 | 1.02 | 0.14 | 2.31 | 0.992 |
| 77 | Qionghai | IG | 542.00 | 0.012 | 1.03 | −0.03 | 2.12 | 0.993 |
| 78 | Sanya | LOGNO | 548.43 | −0.018 | 1.02 | 0.08 | 2.40 | 0.997 |
| 79 | Lingshui | GA | 543.84 | 0.024 | 1.04 | −0.08 | 2.77 | 0.992 |

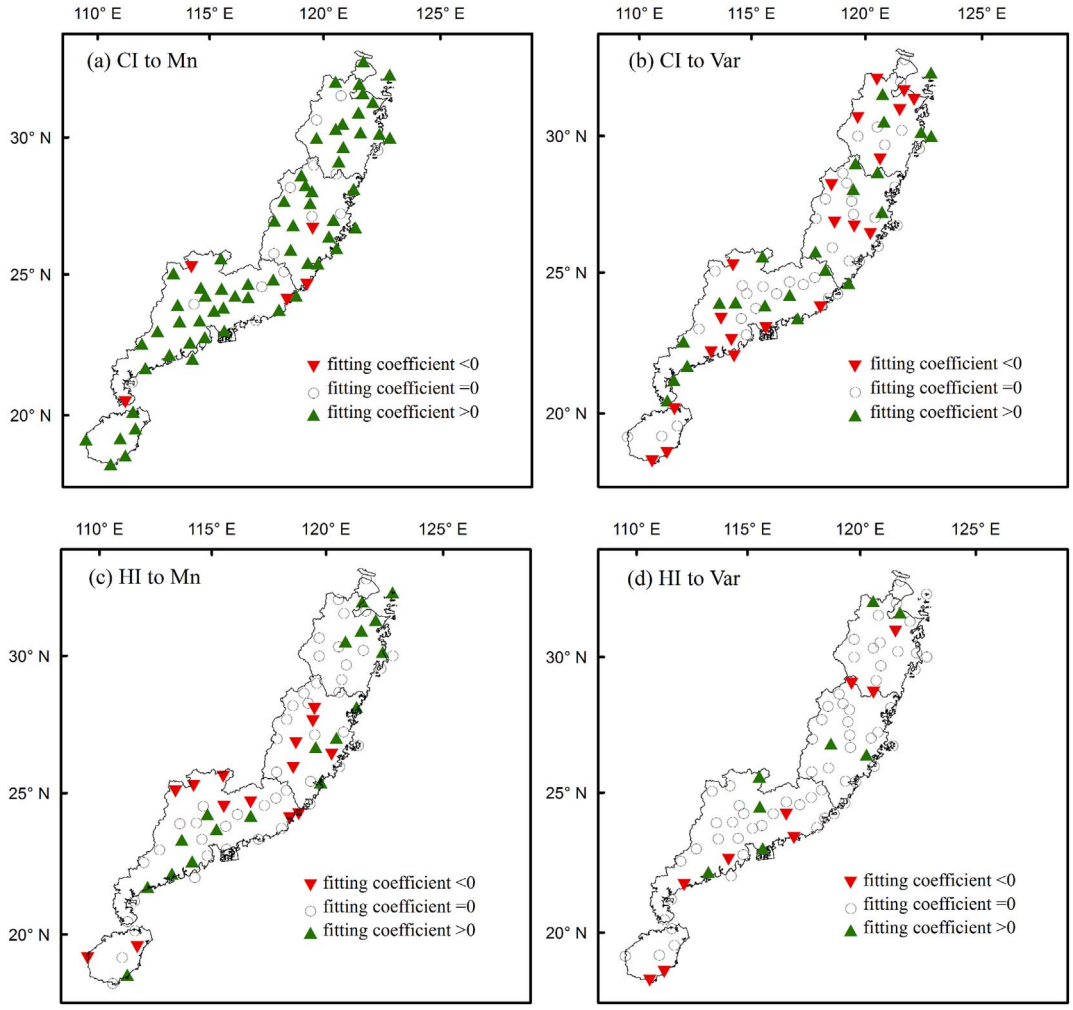


**Fig. 3.** Spatial distribution of the fitting coefficients for CI to Mn and Var (a, b) and HI to Mn and Var (c, d) in GAMLSS.

**Table 4**
Station statistics of the fitting coefficient for Mn and Var of MDP from 1960 to 2012.

| Fitting coefficient | Mn | | Var | |
|---|---|---|---|---|
| | > 0 | < 0 | > 0 | < 0 |
| CI | 60 | 5 | 22 | 20 |
| HI | 18 | 14 | 8 | 9 |

on Mn/Var and vice versa. The positive fitting coefficient at the majority of stations across the entire region (60 stations) shows an increasing impact of CI on Mn (Fig. 3a–b, Table 4). Only five stations have a negative fitting coefficient including two stations (Nos 34 and 61) in Fujian and three stations (Nos 40, 59, and 73) in Guangdong. The fitting coefficient between CI and Var is positive, which indicates an increasing impact of CI. The stations mainly locate in the east of Zhejiang, north and south of Fujian, and east and south of Guangdong. Twenty stations showing decreasing impacts (with negative fitting coefficients) are mainly located in the north of Zhejiang, middle of Fujian, in the coastal region of Guangdong, and in the south of Hainan. The fitting correlation between CI and Var is insignificant in Shanghai, in the middle of Zhejiang and Guangdong, and in the mountain areas (west and middle) of Fujian, with a fitting coefficient value of zero. Generally, CI has more increasing impacts on the Mn and Var trend. Table 4 also demonstrates that CI has influences Mn much more than Var.

Fig. 3c–d show the spatial distribution of the fitting coefficients for HI in GAMLSS. Eighteen stations show a positive fitting coefficient between HI and Mn, which means that HI has an increasing impact on Mn (Table 4). They are mainly located in the north of Zhejiang, in the east of Fujian, and in southern Guangdong. A decreasing impact was found at stations (14 stations) located in the middle of Fujian and north of Guangdong. Two stations are in Hainan (Nos 75 and 77); there are no stations in Zhejiang and Shanghai. Eight and nine stations show decreasing and increasing impacts between HI and Var, respectively. The HI impact is significant in Guangdong, with the most stations (eight stations), compared with other provinces. Two stations (Nos 2 and 5) in

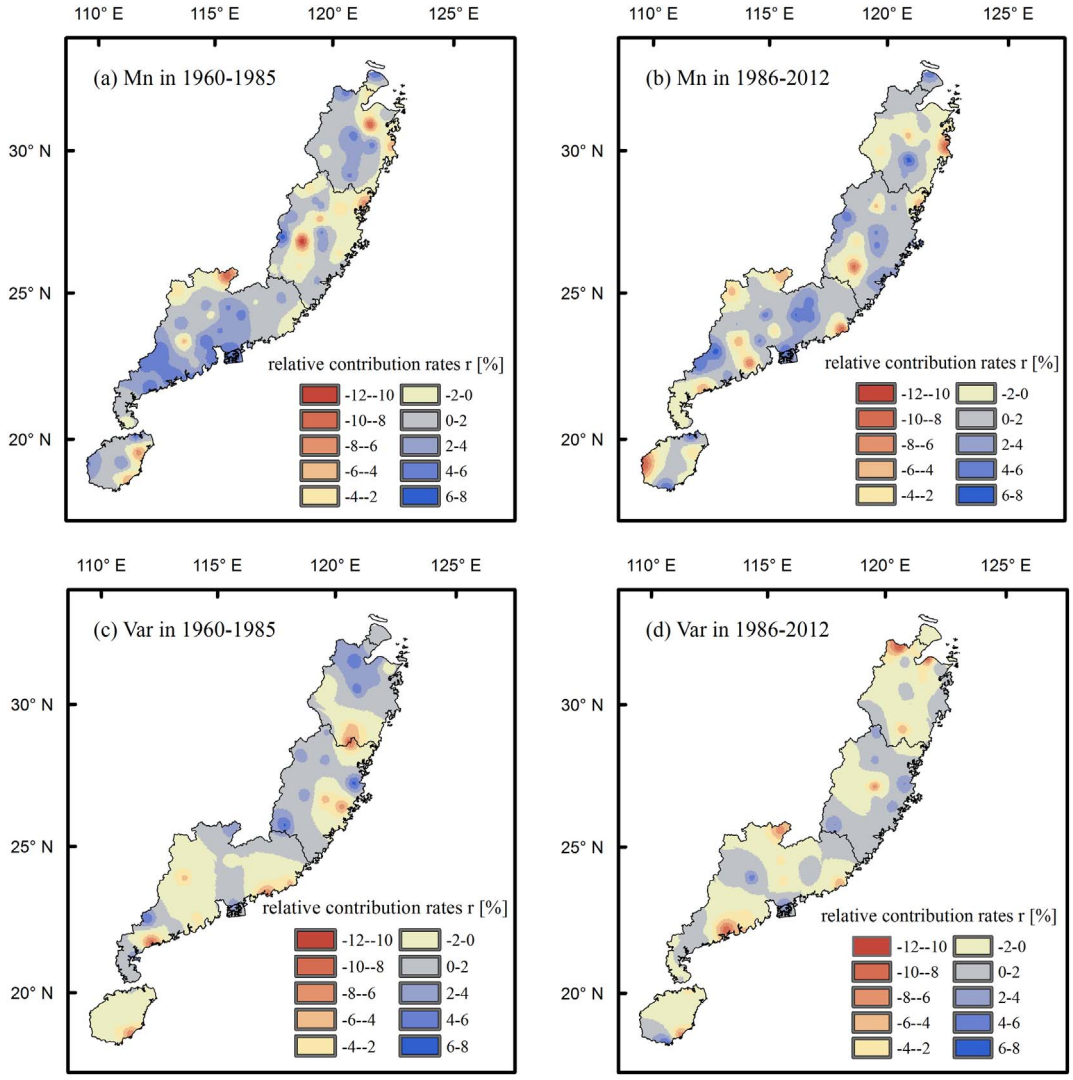


**Fig. 4.** Spatial distribution of the relative contribution rates for Mn (a, b) and Var (c, d) in 1960–1985 and 1986–2012.

the north of Zhejiang and two stations (Nos 32 and 36) in the middle of Fujian have an increasing influence.

### 4.3. Contribution comparison

In the past few decades, China achieved a "leapfrog development" with respect to social and economic development, which represents the strong impact of human activities on climate change. To reveal the intensity of human activities, we divided the time series into two stages: slow socioeconomic development (1960–1985) and rapid socio-economic development (1986–2012). The relative contribution rates (r) of CI and HI to Mn and Var were calculated based on the contribution analysis method. The results were interpolated over the study area for a more direct-view analysis (Fig. 4). A positive rate indicates a greater contribution of CI compared with HI and vice versa. In general, CI contributes more to Mn than Var, while HI affects Var more than Mn. In addition, the contribution of HI to MDP in the stage of rapid socio-economic development (1986–2012) is much more significant than in the stage of slow socioeconomic development (1960–1985), especially in Zhejiang and Guangdong. Specifically, although, the impact of HI on Mn is smaller than that of CI in 1960–1985, its effects are greater in the northeast of Zhejiang, middle and northeast of Fujian, north of Guangdong, and east of Hainan. The CI dominates the Mn changes in the majority of Zhejiang and Guangdong. The situation changes in Fujian because the impact of CI becomes larger in 1986–2012. The impact of HI on Mn also increases from 1986 to 2012 compared with 1960–1985 in Zhejiang and Guangdong. HI contributes more to Var than CI in the coastal region of Guangdong, the majority of Zhejiang and Hainan, and Shanghai City. Fujian has different dominant impact factors in the two phases. From 1986 to 2012, HI significantly impacts Var in the west of Fujian, whereas CI has a greater effect in 1960–1985. Although, the impacts between CI and HI are different, the magnitude of the difference is ~10%.

## 5. Discussion and conclusions

Although the nonstationarity characteristics of extreme precipitation from April to June from 1960 to 2012 are not widespread throughout the southeastern coastal region of China, the trends are significant on local scales. Previous studies have shown similar results in this region. For example, Gao et al. (2016) found 48 of 631 stations show significant nonstationarity for the annual maximum daily precipitation (AMP) series. 25 of 48 stations showing significant positive trend mainly distributed in southern and western China. Different with the above research, the present study focused on the extreme precipitation in April to June rather than AMP. Wang et al. (2017) also found that the extreme precipitation indices (such as number of heavy precipitation days and extremely wet day precipitation) show

increasing trends in the Jiangnan and Huanan coastal area of China. Xiao et al. (2017) indicated that there is a slight wetting tendency but significant intensifying precipitation in southeast China during 1961–2010. However, it is noteworthy that few studies specifically focused on the extreme precipitation in the first flood season.

Fig. 2 shows a stable trend increment of Mn in the north of Zhejiang, middle of Fujian, and south of Guangdong, which indicates that the extreme precipitation increased from 1960 to 2012. The enhanced variability of MDP causes more frequent extreme precipitation events in the north of Zhejiang, middle of Fujian, and coastal region of Guangdong. It is worth noting that Mn and Var both increase in the north of Zhejiang and middle of Fujian (mountain areas), which implies a high risk of extreme precipitation events in these areas. T. Gao et al. (2017) also mentioned that the extreme rainfalls show significant positive trends in the central and south of monsoon regions of China, which indicates the increasing possibility of flood-induced disasters.

Previous studies argued that the combined influence of natural climate change and human activities affects extreme climate events (e.g., IPCC, 2013; Liu et al., 2015). However, most of them focused on the impacts of large-scale circulations. For example, Limsakul and Singhruck (2016) emphasized that large-scale climate phenomena in the Pacific Ocean (such as PDO) are the remote drivers of variability for extreme precipitation in Thailand. T. Gao et al. (2017) also concluded that the Indian Ocean Dipole (IOD), ENSO and Atlantic Multidecadal Oscillation (AMO) have strong impacts on extreme precipitation over monsoon region in China, especially during the 1990s. Zhang et al. (2017) pointed out that the western North Pacific subtropical high (WNPSH) impacts remarkably on precipitation in June in South China. Some other studies applied different variables to represent the climate change such as wind filed and surface sea temperature (SST) (Wang and Zhou, 2005; You et al., 2011). Unfortunately, it is still unclear, which is the main driving force, in particular in different periods. The aerosol and greenhouse gases data is conventional for representing human actives. However, the reservoir information is also possible to represent anthropogenic impacts (Zhang et al., 2015). Compared to previous studies, this study investigated the integrated indices of natural climate change (CI) and human activity (HI) rather than the single factor. It was found that integrated index has a better correlation than any single factor. Therefore, the integrated index reflects not only the comprehensive impact of multiple factors, but also reduces the dimensions of variables in GAMLSS. Overall, the procedure used in this study is more straightforward. The southeastern coastal region has been the fastest developing area since the Chinese Economic Reform and Open Up in the late 1970s. Additionally, with the implementation of special economic zones and “the Silk Road Economic Belt and 21st Century Maritime Silk Road”, this region will maintain the rapid development characterized by high-speed urbanization in the future. Based on statistics, the urban area of these five provinces (city) accounts for 22.3% continent of China (Wang et al., 2013). The land use/land cover change would lead to changes of micrometeorological characteristics, such as albedo, evapotranspiration, and heat island effect, which further influence the local climate. In general, human activities become more and more intense. Regions with larger human activities often show higher urbanization levels (Fig. 4). Therefore, it is necessary to investigate the impact of the natural climate change and human activity on extreme precipitation events.

The natural climate change is responsible for the Mn increment in the entire period of 1960–2012 (Fig. 3). The stations have the increasing impacts of climate change on Var is almost numerically equal to the ones have decreasing impacts (22 to 20 stations). In 1960–2012, human activity did not show a dominant impact on Mn and Var (Table 4). However, Fig. 4 clearly shows contribution differences of these two impact factors in different periods. Human activities cause more variability, especially in 1986–2012 (Fig. 4c and d), while natural climate changes lead to a higher mean climate state, especially in 1960–1985 (Fig. 4a and b). In consequence, more extreme precipitation events are possibly triggered by a slightly increased variance, even when the climate is in an invariable mean state. Therefore, the community should pay more attention to the possibility of extreme precipitation events and its associated disasters triggered due to human activities.

To better distinguish the impact between natural climate change and human activities, we utilized CI and HI instead of directly using all variables in GAMLSS. However, this procedure might introduce issues. Firstly, the CI and HI are arbitrary to some extent because they are obtained using statistical relationships based on PCA rather than physical mechanisms. These selected variables are not always linearly correlated with extreme precipitation. Secondly, it is possible that GAMLSS could perform very well when directly using the circulation indices and emission variables because it is capable of identifying the most correlated variables with extreme precipitation trends (e.g., Villarini et al., 2010; Zhang et al., 2015; L. Gao et al., 2017). Thirdly, we chose the year of 1985 as the demarcation point to distinguish the strength of human activities based on the socioeconomic development. This selection is possibly problematic because a changepoint of the extreme series might cause significant increase or decrease (Zhang et al., 2014). Lu et al. (2012) pointed out that there was a significant increasing trend of extremely heavy precipitation events in summer half year in South China from mid-1980s. Zhang et al. (2014) also found that the annual peak flood (APF) which closely connected to precipitation abrupt changed in some water reservoirs (like Baipenzhu) in Pearl River basin in Guangdong Province in mid-1980s. L. Gao et al. (2017) found that the extreme precipitation of 26 stations during the second flood season in the Southeastern Coastal Region of China show change points in the mid of 1980s, especially around 1987. Furthermore, in 1978, the Third Plenary Session of the Eleventh Central Committee of the Communist Party of China established the national policy of Economic Reform and Open Up. Four cities, Shenzhen, Zhuhai, Xiamen and Shantou in 1979 and other 14 port cities in 1984 were selected as the experimental cities for the new economic policy. However, the establishment of Special Economic Zones (Yangtze River Delta, Pearl River Delta, Southeast Fujian and Bohai Economic Rim) in 1985 indicates that the regional socioeconomic has entered a period of fast growth. Based on the above reasons, the present study chose the year of 1985 to divide the different socioeconomic development stages. Moreover, other relative variables, such as wind fields at pressure level, SST, aerosol and terrain, and underlying surface characteristics, should be considered. Finally, this analysis needs to be extended to more physical mechanisms. Due to the limitations of the GAMLSS model, the present work focuses more on statistical characteristics analysis.

Nonstationarity characteristics of extreme precipitation are analyzed in this study, considering the impact of both climate change and human activity during the first flood season in the southeastern coastal region of China. Overall, this work provides general insights into the impact of natural climate change (non-anthropogenic) and human activity (anthropogenic) on extreme precipitation. The results show that nonstationarity is significant on local scales. Natural climate change has a great impact on the mean state of extreme precipitation, while human activity leads to significant variability. Furthermore, the contribution of human activity to Var is much more significant than that of natural climate change with a difference of ~10%. It is also more significant in the stage of rapid socioeconomic development (1986–2012) than in the stage of slow socioeconomic development (1960–1985). To the best of our knowledge, this is the first quantitative assessment for the contributions of natural climate change and human activities to the trend of extreme precipitation in the southeastern coastal region of China. However, we expect more researches to improve the methodology of assessment and to test more influencing factors in the future.

## Acknowledgments

This study was supported by National Natural Science Foundation of

China [grant number 41501106], National Social Science Foundation of China [grant number 14ZDB151], Scientific Projects from the Fujian Provincial Department of Science & Technology [grant number 2015J05080], and Scientific Research Foundation for Returned Scholars, Ministry of Education of China [grant number 2014-1685]. The meteorological data have been provided by China Meteorological Data Sharing Service System of National Meteorological Information Center (http://data.cma.cn/). The large-scale circulation parameters are provided by the Climate Diagnostics and Prediction Division of the National Climate Center of China (http://ncc.cma.gov.cn). The greenhouse gases emission data is provided by the Emission Database for Global Atmospheric Research (EDGAR v4.2) in the Joint Research Center of the European Commission (http://edgar.jrc.ec.europa.eu/overview.php?v=42).

## References

Alexander, L.V., Zhang, X.B., Peterson, T.C., Caesar, J., Gleason, B., Klein Tank, A.M.G., Haylock, M., Collins, D., Trewin, B., Rahimzadeh, F., 2006. Global observed changes in daily climate extremes of temperature and precipitation. J. Geophys. Res. 111 (D05109). http://dx.doi.org/10.1029/2005JD006290.

Beguería, S., Angulo-Martínez, M., Vicente-Serrano, S.M., López-Moreno, J.I., El-Kenawy, A., 2011. Assessing trends in extreme precipitation events intensity and magnitude using non-stationary peaks-over-threshold analysis: a case study in northeast Spain from 1930 to 2006. Int. J. Climatol. 31 (14), 2102–2114. http://dx.doi.org/10.1002/joc.2218.

Chan, J.C.L., Zhou, W., 2005. PDO, ENSO and the early summer monsoon rainfall over south China. Geophys. Res. Lett. 32 (L08810). http://dx.doi.org/10.1029/2004gl022015.

Coumou, D., Rahmstorf, S., 2012. A decade of weather extremes. Nat. Clim. Chang. 2 (7), 491–496. http://dx.doi.org/10.1038/nclimate1452.

Ding, Y.H., 2008. Human activity and the global climate change and its impact on water resources. ChinaWater Resour. 2, 20–27 (in Chinese).

Du, Y., Yang, L., Xie, S.P., 2011. Tropical Indian ocean influence on northwest pacific tropical cyclones in summer following strong El Nino. J. Clim. 24 (1), 315–322. http://dx.doi.org/10.1175/2010JCLI3890.1.

Easterling, D.R., Evans, J.L., Groisman, P.Y., Karl, T.R., Kunkel, K.E., Ambenje, P., 2000. Observed variability and trends in extreme climate events: a brief review. Bull. Am. Meteorol. Soc. 81 (3), 417–425. http://dx.doi.org/10.1175/1520-0477(2000)081<0417:Ovatie>2.3.Co;2.

Fischer, E.M., Knutti, R., 2015. Anthropogenic contribution to global occurrence of heavy-precipitation and high-temperature extremes. Nat. Clim. Chang. 5 (6), 560–564. http://dx.doi.org/10.1038/nclimate2617.

Fu, C.B., 2003. Potential impacts of human-induced land cover change on East Asia monsoon. Glob. Planet. Chang. 37 (3–4), 219–229. http://dx.doi.org/10.1016/S0921-8181(02)00207-2.

Fu, G.B., Yu, J.J., Yu, X.B., Ouyang, R.L., Zhang, Y.C., Wang, P., Liu, W.B., Min, L.L., 2013. Temporal variation of extreme rainfall events in China, 1961–2009. J. Hydrol. 487, 48–59. http://dx.doi.org/10.1016/j.jhydrol.2013.02.021.

Gao, X.J., Zhao, Z.C., Giorgi, F., 2002. Changes of extreme events in regional climate simulations over East Asia. Adv. Atmos. Sci. 19 (5), 927–942. http://dx.doi.org/10.1007/s00376-002-0056-2.

Gao, M., Mo, D., Wu, X., 2016. Nonstationary modeling of extreme precipitation in China. Atmos. Res. 182, 1–9. http://dx.doi.org/10.1016/j.atmosres.2016.07.014.

Gao, L., Huang, J., Chen, X.W., Chen, Y., Liu, M.B., 2017. Risk of extreme precipitation under nonstationarity conditions during the second flood season in the southeastern coastal region of China. J. Hydrometeorol. 18 (3), 669–681. http://dx.doi.org/10.1175/JHM-D-16-0119.1.

Gao, T., Wang, H.J., Zhou, T., 2017. Changes of extreme precipitation and nonlinear influence of climate variables over monsoon region in China. Atmos. Res. 197, 379–389. http://dx.doi.org/10.1016/j.atmosres.2017.07.017.

Gilroy, K.L., McCuen, R.H., 2012. A nonstationary flood frequency analysis method to adjust for future climate change and urbanization. J. Hydrol. 414-415 (2), 40–48. http://dx.doi.org/10.1016/j.jhydrol.2011.10.009.

Gu, X.H., Zhang, Q., Kong, D., Liu, J., 2016. Nonstationarity of flooding processes in the Tarim River Basin and climate-related impacts. J. Nat. Resour. 31, 1499–1513. http://dx.doi.org/10.11849/zrzyxb.20151164. (in Chinese).

Ingram, W., 2016. Extreme precipitation: increases all round. Nat. Clim. Chang. 6 (5), 443–444. http://dx.doi.org/10.1038/nclimate2966.

IPCC, 2013. Climate Change 2013: The Physical Science Basis. Cambridge University Press, Cambridge. http://dx.doi.org/10.1017/CBO9781107415324.

Karl, T.R., Knight, R.W., 1998. Secular trends of precipitation amount, frequency, and intensity in the United States. Bull. Am. Meteorol. Soc. 79 (2), 231–241. http://dx.doi.org/10.1175/1520-0477(1998)079<0231:STOPAF>2.0.CO;2.

Katz, R.W., Brown, B.G., 1992. Extreme events in a changing climate: variability is more important than averages. Clim. Chang. 21 (3), 289–302. http://dx.doi.org/10.1007/BF00139728.

Khaliq, M.N., Ouarda, T.B.M.J., Ondo, J.C., Gachon, P., Bobée, B., 2006. Frequency analysis of a sequence of dependent and/or non-stationary hydro-meteorological observations: a review. J. Hydrol. 329 (3–4), 534–552. http://dx.doi.org/10.1016/j.jhydrol.2006.03.004.

Limsakul, A., Singhruck, P., 2016. Long-term trends and variability of total and extreme precipitation in Thailand. Atmos. Res. 169, 301–317. http://dx.doi.org/10.1016/j.atmosres.2015.10.015.

Liu, J.Y., Shao, Q.Q., Yan, X.D., Fan, J.W., Deng, X.Z., Zhan, J.Y., 2011. An overview of the progress and research framework on the effects of land use change upon global climate. Adv. Earth Science 26 (10), 1015–1022 (in Chinese).

Liu, R., Liu, S.C., Cicerone, R.J., Shiu, C.J., Li, J., Wang, J.L., Zhang, Y.H., 2015. Trends of extreme precipitation in eastern China and their possible causes. Adv. Atmos. Sci. 32 (8), 1027–1037. http://dx.doi.org/10.1007/s00376-015-5002-1.

Lu, H., Chen, S.R., Guo, Y., He, H., Xu, S.X., 2012. Spatio-temporal variation characteristics of extremely heavy precipitation frequency over South China in the last 50 years. J. Trop. Meteorol. 28 (2), 219–227. http://dx.doi.org/10.3969/j.issn.1004-4965.2012.02.009. (in Chinese).

Mearns, L.O., Katz, R.W., Schneider, S.H., 1984. Extreme high-temperature events: changes in their probabilities with changes in mean temperature. J. Clim. Appl. Meteorol. 23 (12), 1601–1613. http://dx.doi.org/10.1175/1520-0450(1984)023,1601:EHTECI.2.0.CO;2.

Milly, P.C., Betancourt, J., Falkenmark, M., Hirsch, R.M., Kundzewicz, Z.W., Lettenmaier, D.P., Stouffer, R.J., 2008. Climate change. Stationarity is dead: whither water management? Science 319 (5863), 573–574. http://dx.doi.org/10.1126/science.1151915.

Min, S.K., Zhang, X., Zwiers, F.W., Hegerl, G.C., 2011. Human contribution to more-intense precipitation extremes. Nature 470 (7334), 378–381. http://dx.doi.org/10.1038/nature09763.

Ning, L., Qian, Y.F., 2009. Interdecadal change in extreme precipitation over south China and its mechanism. Adv. Atmos. Sci. 26 (1), 109–118. http://dx.doi.org/10.1007/s00376-009-0109-x.

Ohba, M., 2013. Important factors for long-term change in ENSO transitivity. Int. J. Climatol. 33 (6), 1495–1509. http://dx.doi.org/10.1002/joc.3529.

Ohba, M., Kadokura, S., Yoshida, Y., Nohara, D., Toyoda, Y., 2015. Anomalous weather patterns in relation to heavy precipitation events in Japan during the baiu season. J. Hydrometeorol. 16 (2), 688–701. http://dx.doi.org/10.1175/Jhm-D-14-0124.1.

Qin, D.H., Ding, Y.H., Su, J.L., Wang, S.M., 2005. Climate and environment changes in China. In: Climate and Environment Changes in China and Their Projects. vol. 1 Science Press, Beijing (in Chinese).

Rigby, R.A., Stasinopoulos, D.M., 2005. Generalized additive models for location, scale and shape. J. Royal Stat. Soc 54C (3), 507–554. http://dx.doi.org/10.1111/j.1467-9876.2005.00510.x.

Rigby, B., Stasinopoulos, M., 2009. A Flexible Regression Approach Using GAMLSS in R. University of Lancaster (November 13, 2009).

Rosenfeld, D., Lohmann, U., Raga, G.B., O'Dowd, C.D., Kulmala, M., Fuzzi, S., Reissell, A., Andreae, M.O., 2008. Flood or drought: how do aerosols affect precipitation? Science 321 (5894), 1309–1313. http://dx.doi.org/10.1126/science.1160606.

Salazar, A., Baldi, G., Hirota, M., Syktus, J., McAlpine, C., 2015. Land use and land cover change impacts on the regional climate of non-Amazonian South America: a review. Glob. Planet. Chang. 128, 103–119. http://dx.doi.org/10.1016/j.gloplacha.2015.02.009.

Song, D., Cai, S., 2007. China Meteorological disasters: Fujian. China Meteorological Press, Beijing (in Chinese).

Villarini, G., Smith, J.A., Napolitano, F., 2010. Nonstationary modeling of a long record of rainfall and temperature over Rome. Adv. Water Resour. 33 (10), 1256–1267. http://dx.doi.org/10.1016/j.advwatres.2010.03.013.

Wan, S.Q., Hu, Y.L., You, Z.Y., Kang, J.P., Zhu, J.G., 2013. Extreme monthly precipitation pattern in China and its dependence on Southern Oscillation. Int. J. Climatol. 33 (4), 806–814. http://dx.doi.org/10.1002/joc.3466.

Wang, Y., 2015. Air pollution or global warming: attribution of extreme precipitation changes in eastern China-comments on "Trends of extreme precipitation in eastern China and their possible causes". Adv. Atmos. Sci. 32 (10), 1444–1446. http://dx.doi.org/10.1007/s00376-015-5109-4.

Wang, Y.Q., Zhou, L., 2005. Observed trends in extreme precipitation events in China during 1961–2001 and the associated changes in large-scale circulation. Geophys. Res. Lett. 32 (9). http://dx.doi.org/10.1029/2005gl022574.

Wang, J.A., Zhou, H.J., Yuan, Y., Shi, P.J., 2013. Regional Disaster Dystem and Risk Prevention Mode of Typhoon Disaster Chain: A Case Study of Guangdong. China Environmental Science Press, Beijing (in Chinese).

Wang, X., Hou, X., Wang, Y., 2017. Spatiotemporal variations and regional differences of extreme precipitation events in the Coastal area of China from 1961 to 2014. Atmos. Res. 197, 94–104. http://dx.doi.org/10.1016/j.atmosres.2017.07.017.

Xiao, M., Zhang, Q., Singh, V.P., 2017. Spatiotemporal variations of extreme precipitation regimes during 1961–2010 and possible teleconnections with climate indices across China. Int. J. Climatol. 37 (1), 468–479. http://dx.doi.org/10.1002/joc.4719.

Xie, S.P., Hu, K.M., Hafner, J., Tokinaga, H., Du, Y., Huang, G., Sampe, T., 2009. Indian ocean capacitor effect on Indo-Western Pacific climate during the summer following El Nino. J. Clim. 22 (3), 730–747. http://dx.doi.org/10.1175/2008JCLI2544.1.

Xu, X., Du, Y.G., Tang, J.P., Wang, Y., 2011. Variations of temperature and precipitation extremes in recent two decades over China. Atmos. Res. 101 (1–2), 143–154. http://dx.doi.org/10.1016/j.atmosres.2011.02.003.

You, Q.L., Kang, S.C., Aguilar, E., Pepin, N., Flugel, W.A., Yan, Y.P., Xu, Y.W., Zhang, Y.J., Huang, J., 2011. Changes in daily climate extremes in China and their connection to the large scale atmospheric circulation during 1961–2003. Clim. Dyn. 36 (11−12), 2399–2417. http://dx.doi.org/10.1007/s00382-009-0735-0.

Zhai, P.M., Zhang, X.B., Wan, H., Pan, X.H., 2005. Trends in total precipitation and frequency of daily precipitation extremes over China. J. Clim. 18 (7), 1096–1108. http://dx.doi.org/10.1175/Jcli-3318.1.

Zhang, Q., Xu, C.Y., Zhang, Z.X., Chen, Y.D., Liu, C.L., Lin, H., 2008. Spatial and temporal

variability of precipitation maxima during 1960–2005 in the Yangtze River basin and possible association with large-scale circulation. J. Hydrol. 353 (3–4), 215–227. http://dx.doi.org/10.1016/j.jhydrol.2007.11.023.

Zhang, Q., Xu, C.Y., Zhang, Z., Chen, Y.D., Liu, C.L., 2009. Spatial and temporal variability of precipitation over China, 1951–2005. Theor. Appl. Climatol. 95 (1–2), 53–68. http://dx.doi.org/10.1007/s00704-007-0375-4.

Zhang, Q., Gu, X.H., Singh, V.P., Xiao, M.Z., Xu, C.Y., 2014. Stationarity of annual flood peaks during 1951–2010 in the Pearl River basin, China. J. Hydrol. 519 (D), 3263–3274. http://dx.doi.org/10.1016/j.jhydrol.2014.10.028.

Zhang, Q., Gu, X.H., Singh, V.P., Xiao, M.Z., Chen, X.H., 2015. Evaluation of flood frequency under non-stationarity resulting from climate indices and reservoir indices in the East River basin, China. J. Hydrol. 527, 565–575. http://dx.doi.org/10.1016/j.jhydrol.2015.05.029.

Zhang, Q., Zheng, Y., Singh, V.P., Luo, M., Xie, Z., 2017. Summer extreme precipitation in eastern China: mechanisms and impacts. J. Geophys. Res. 122 (5), 2766–2778. http://dx.doi.org/10.1002/2016JD025913.